Published in final edited form as:

Cell Mol Bioeng. 2015 December ; 8(4): 553–565. doi:10.1007/s12195-015-0395-6.

EGF as a New Therapeutic Target for Medulloblastoma Metastasis

Jennifer Rico-Varela[1,#], **Tanya Singh**[1,#], **Sean McCutcheon**[1], and **Maribel Vazquez**[1,*]

[1]Department of Biomedical Engineering, The City College of New York, 160 Convent Avenue, ST-403D, New York, NY 10031

Abstract

Medulloblastoma (MB) is a malignant pediatric brain tumor known for its aggressive metastatic potential. Despite the well-documented migration of MB cells to other parts of the brain and spinal column, MB chemotaxis is poorly understood. Herein, we examined the *in vitro* migratory and cellular responses of MB-derived cells to external signaling of Epidermal Growth Factor (EGF), hepatocyte growth factor (HGF), platelet-derived growth factor (PDGF-BB), and the stromal cell-derived factors 1-alpha (SDF-1). Experiments utilized transwell assays and immunocytochemistry to identify receptor activation in MB migration, and used a microfluidic platform to examine directionality, trajectory, and gradient-dependence of motile cells. Data illustrates that MB-derived cells respond strongly to EGF in a dosage and gradient-dependent manner with increased EGF-R activation, and show that high EGF gradient fields cause an increased number of cells to migrate longer directed distances. Our results provide evidence that EGF and its receptor play an important role than previously documented in MB chemotactic migration than previously documented and should be considered for developing migration-target therapies against MB metastasis.

Keywords

Pediatric cancer; chemotaxis; microfluidics; gradients

INTRODUCTION

Medulloblastoma (MB) is a family of highly-invasive tumors most commonly diagnosed in the pediatric central nervous system [7, 28, 38, 41, 50]. While clinical treatments have more

* Corresponding author. The City College of The City University of New York, New York, NY vazquez@ccny.cuny.edu.
# Co-first authors
jrico00@citymail.cuny.edu
tsingh09@citymail.cuny.edu
smccutc00@citymail.cuny.edu

CONFLICTS OF INTEREST:
Jennifer Rico-Varela, declares that she has not conflicts of interest.
Tanya Singh, declares that she has not conflicts of interest.
Sean McCutcheon, declares that he has not conflicts of interest.
Dr. Maribel Vazquez, declares that she has not conflicts of interest.

ETHICAL STANDARDS:
No human studies were carried out by the authors for this article.
No animal studies were carried out by the authors for this article.

than doubled the overall 5-year survival rate to upwards of 60% [16, 28, 44, 52], additional therapies are needed to target the aggressive MB migration that is uncharacteristic of other brain tumors, but is a hallmark of MB recurrence, metastasis, and radioresistivity [13, 21, 24, 28, 41, 55, 61, 70]. The migration of cancer cells within the CNS is decidedly complex, affected by cellular interactions with heterogeneous extracellular matrix (ECM) as well as mixed cellular responses to concentration fields of biomolecules [1, 14, 19, 60, 65]. However, the mechanisms behind the migration of MB-derived cells along CNS gradients of biomolecular concentration, or chemotaxis, remain understudied and incompletely understood [14, 28]. Particular complexities arise in MB, because chemoattractant fields that rouse cells away from primary tumors can be secreted by healthy or transformed distant and neighboring cells [1, 3, 9, 34, 58, 76]. Further, clinical studies have illustrated that the spread of MB cells occurs predominantly to the spinal column via a combination of two-dimensional (2D) and three-dimensional (3D) movements [6, 51, 67, 77, 83]. Such spreading results from tumor cells that drop into the cerebrospinal fluid and tend to seed in parts of the spine [53, 74, 77, 79, 84]. As a result, the movement of MB cells on the surface of the spinal column can be examined on 2D substrata to plausibly physiologically approximate the metastatic behavior of these pediatric brain tumors.

Traditional cell migration studies have looked to transwell [27, 48, 81] and wound healing assays [36, 54, 78] to report numbers of cells that become motile in response to external signaling from growth factors, such as Epidermal Growth Factor (EGF) and Platelet-Derived Growth Factor (PDGF) [4]. However, chemotaxis is becoming more-commonly examined via the physical microenvironment of the cell, where dynamic concentration fields facilitate ligand-receptor bindings which initiate signal transduction cascades [1, 8, 59]. Here, precise manipulation of the cell microenvironment has been facilitated by the wide-adaptation of benchtop microfluidic devices [26, 27, 29], which enable multifaceted evaluation of cell migratory behaviors in lieu of cell numbers alone. A large number of laboratories have demonstrated concentration- and concentration gradient-dependent behavior of non-cancerous cells, such as fibroblasts [33], retinal progenitor cells [69] and keratinocytes [64], as well as tumors found in breast [57], colon [17] and CNS cancers [2]. Our own laboratory has illustrated that select populations of cells derived from CNS tumors can respond acutely via migration to ultra-low concentration gradients of select chemoattractants [2, 14, 33], while others have shown greater chemotactic response with specific dosage [3, 49, 56]. Microfluidic analysis is, thus, well positioned to meaningfully aid in the development of migration-targeted therapies for MB via insight of migratory parameters relevant to metastasis, such as cell distance traveled, motility, gradient-sensitivity, ECM interaction and numerous others.

In this work, we examine MB migratory behavior in response to external signaling from 4 of the most extensively studied chemoattractants of CNS tumors using benchtop assays and microfluidics: Epidermal Growth Factor (EGF), Platelet-derived Growth Factor (PDGF), Hepatocyte Growth Factor (HGF), and Stromal Derived Growth Factor (SDF-1 or CXCL12). Our results illustrate that MB-derived cells exhibit gradient-dependent behavior in EGF fields, which are able to guide MB along longer migration distances with superior directionality and increased receptor activation. These results distinguish EGF as a principal

molecule with meaningful potential impact as an anti-migratory therapeutic to MB metastasis.

MATERIALS AND METHODS

Cell culture

In vitro cell culture was maintained using Daoy cell line (ATCC, Cat. No.HTB-186) [14, 60], Eagle's Minimal Essential Medium (EMEM) (VWR, Cat. No.12001-582) supplemented with 10% fetal bovine serum (VWR, Cat. No.45000-734), 2% L-glutamine (VWR, Cat. No. 45000-676) and 1% Penicilin-Streptomycin (VWR, Cat. No.45000-650). Intact monolayers were maintained and harvested cells were seeded onto sterile polystyrene tissue culture flasks (VWR, Cat. No.BD353136). MB cells were incubated at 37 °C with 5% CO_2 with cell medium changed every 2 days. Cell migration experiments were initiated with cells that were inserted into microchannel after MB cells reached 80% confluence.

Cell Migration Assay

The Boyden chamber assay [2, 14] was used to measure the number of MB cells that migrated towards different concentrations of external growth factors. This widely-used assay consists of two compartments filled with EMEM medium and separated by an 8 micron-porous membrane (VWR, Cat. No.62406-198), as shown in Figure 1.A. MB cells were seeded in the upper compartment and were allowed to migrate through the porous membrane into the lower compartment for 6 hours at 37 °C in a 5% CO_2 incubator. Approximately 1×10^6 cells/mL were seeded in 300μl of EMEM complete medium (EMEM with FBS) in each upper chamber, while 700μl of serum-free medium (EMEM only) was pipetted into each lower chamber. Lower chambers also contained concentrations of 1, 10, 100, and 1000 ng/mL of EGF (Life Technologies Corporation, Cat. No.E3476); HGF (R&D Systems, Cat. No.2207-HG/CF); PDGF-BB (R&D Systems, Cat. No.220-BB-010); and finally SDF-1 (PreporTech, Cat. No.250-20A). All growth factor solutions were diluted in EMEM serum-free medium using serial dilution. After 6 hours of incubation, the membrane was fixed and stained with fixative solutions (VWR, Cat. No. B4132-11A), which stained the cell cytoplasm and nuclei. The number of cells that migrated to the underside of each membrane was determined by using the convectional checkerboard analysis [2, 14, 82].

Immunostainning of Receptors

MB cells were plated at a concentration of 1×10^3 cells/mL in EMEM complete, on borosilicate glass well plates (Lab-Tek, Cat. No.155383). The cells were incubated for 2 hours at 37°C in 5% CO_2 to facilitate attachment. Adhered cells were exposed to ligands at concentrations that resulted in the largest numbers of motile cells in the transwell assay results. At 37°C, each cell plate was exposed to 5 minutes of: 100ng/mL EGF (Life Technologies, Cat. No.PGH0311), 100ng/mL CXCL12 (Life Technologies, Cat. No.PHC1364), 10ng/mL HGF (Life Technologies, Cat. No.PHG0324), and 100ng/mL PDGF-BB (Life Technologies, Cat. No.PHG0044). The supernatant was then aspirated and each well was rinsed 3 times with 0.5 mL phosphate buffered saline solution (PBS), (Sigma-Aldrich, Cat. No.D8537). Each well was fixed using 10% paraformaldehyde (Sigma-Aldrich, Cat. No.HT501128) for 10 minutes, and rinsed twice with PBS. The samples were

permeabilized using a 1% solution of Triton-X (Sigma-Aldrich, Cat. No.X100) and 0.1%BSA in PBS solution for 10 minutes, then blocked for 60 minutes with 1% BSA in PBS blocking solution and rinsed twice with the same blocking solution.

Samples were then exposed to the primary antibody for each receptor studied for 2 hours at 22°C: 5μg/mL anti-EGFR (Life Technologies, Cat. No.700308), 5μg/mL anti-CXCR4 (Life Technologies, Cat. No.35-8800), 2μg/mL anti-c-Met (Millipore, Cat. No.072242), and 3μg/mL anti-PDGFR (Life Technologies, Cat. No.701142). Each well was rinsed 3 times with 1% BSA blocking solution. A fluorescent secondary anti-rabbit IgG (Millipore, Cat. No.AP132F) was used for EGFR, c-Met, and PDGFR samples, and a fluorescent anti-mouse secondary antibody (Millipore, Cat. No.MAB1976) was used for CXCR4 samples. All samples were exposed to the secondary antibody at a concentration of 5μg/mL for 30 minutes at 22°C, and then rinsed twice with blocking solution. Nuclear staining (Life Technologies, Cat. No.R37605) was performed for 20 minutes at 22°C, after which the samples were rinsed twice with PBS and covered in glycerol (Life Technologies, Cat. No. 15514-011) for preservation. In addition, the expression of EGFR was measured at different time points of 0, 14, 22, 36, and 42 hours. The immunocytochemistry assay was performed as described above using goat-anti mouse IgG secondary antibody (Life Technologies, Cat. No. A-11005) for EGFR.

Bridged *μ*Lane and Experimental Set up

Our microfluidic device, the *μ*Lane, was utilized to image the real-time migratory responses of individual MB cells within microenvironments of defined EGF and SDF-1 gradient profiles. The bridged *μ*Lane system operates via a combination of uniaxial bulk convection and diffusion to achieve controlled chemical concentration gradients over time, as described previously [2, 32, 33]. This mass transfer mechanism termed as convective-diffusion has been widely-studied by several groups for bioengineering applications, to determine the transport of differently sized solutes and proteins through the walls of capillaries [11, 12, 20] and arteries [25, 30, 39, 66, 80], skeletal muscle fibers [31, 35, 45], and intervertebral discs [18, 62, 63]. The two-dimensional mass transport of ligands within the microsystem was modeled via finite-element-analysis (FEM) in Matlab 7.7 (MathWorks, Natick, MA) and verified experimentally as described previously by our group [32, 33].

The framework of the *μ*Lane system consists of two layers of Polydimethylsiloxame (PDMS) (Fisher Scientific, Cat. No.NC9644388) bonded to a glass slide using ozone gas. The first layer of PDMS consists of a closed microchannel of 100μm-width and 1.3cm-length with a volume of 0.1μL, which connects two fluidic reservoirs of 9μL each, called the source (SRR) and the sink (SKR) reservoir. The second layer of PDMS consists of two chambers of 170μL each, called the source (SRC) and the sink (SKC) chamber, connected by an open, hemispherical bridge channel to maintain the hydrostatic equilibrium of the system [32, 33, 69]. Both chambers are vertically and fluidically connected with both reservoirs (Figure 3).

The *μ*Lane system works by using the larger volumes of the SRC, SKC and bridge channel on the second layer of PDMS to generate concentration gradients within the smaller volumes of the SRR, SKR and microchannel on the first layer [14, 32, 33, 69]. After inserting cells

along the microchannel length, the cell culture media is used to fill the SRR, SKR, SRC, SKC, and the bridge channel. The ligand solutions (EGF or SDF-1) are then manually inserted drop-wise into the SRC until the solution makes contact with the cell culture media solution within the bridge channel and SKC to initiate the molecular transport within the system. The small differences in the density of the reagents and in the liquid levels in the SRR and SKR generate hydrostatic pressure differences that initiate an ultra-low bulk flow within the microchannel in the first layer [32, 33, 69]. This minuscule bulk flow was measured to be 0.37 μm/sec using fluorescent beads, as described previously [32]. Such a low bulk flow facilitates the transport of ligand solutions from the SRR to the SKR, to accelerate the time required to attain a steady-state gradient profile of ligand solutions along the 13-mm length of the microchannel. In the absence of this bulk flow, the transport of our reagent via diffusion alone would require over 470 hours to reach a steady-state distribution within the length of the *μ*Lane instead of the 18 hours measured, as reported by our group [14, 32]. We note that because the time required for the overall system to reach steady-state is much larger than the time needed for steady-state concentration gradients to be generated within the *μ*Lane system alone. Thus, the operation of the system is 'best' described as 'quasi-steady-state' [5, 10, 40, 68, 71, 73]. However, because this work focuses exclusively on smaller time scales of the microchannel only, the term steady-state would be used for simplicity. Mathematical models of reagent transport within our *μ*Lane system were performed via MatLab to determine the steady-state concentration distribution as seen in Figure 4.A. The initial EGF or SDF-1 concentration within the SKC, SKR, microchannel and SRR was set to 0-ng/mL, as per absence of ligand. The initial ligand concentration within the SRC was set to 100-ng/mL to reflect the sample concentration used during experiments. These boundary conditions were solved using Equation **(1)**, as shown below [32],

$$\frac{\partial C}{\partial t} + \underline{u} \cdot \underline{\nabla} C = D \nabla^2 C \quad (1)$$

Where C (ng/mL) is ligand concentration, t (hours) is time, u (μm/sec) is fluid velocity, and D (cm^2/s) is diffusion coefficient, or diffusivity, of the reagent molecule. Experimental validation was also performed using fluorescently labeled Dextran (~ MW 10KDa), to confirm steady-state is reached in our system after 18 hours, and is maintained for several days [14, 32].

For our experiments, the *μ*Lane system was coated with 10-μg/mL of laminin (Becton, Dickinson and Company, Cat. No.354232) [14, 60], and allowed to gel for one hour at room temperature (25°C) under sterile conditions. Unbound laminin was aspirated and cells were manually seeded into the microchannel using a 1-mL syringe (VWR, Cat. No.BD309659). A cell solution (1×10^6 cells/mL) was injected into the SRR and SKR. Cells were allowed to adhere and visibly spread prior to the initiation of the experiment as illustrated in Figure 3.D. Finally the bridge channel was loaded with EMEM complete medium to connect the SRC and SKC, initiating the system. In this work, EGF (100-ng/mL) or SDF-1 (100-ng/mL) was individually loaded drop-wise into the SRC and allowed to reach steady state in the microchannel for 18 hours at 37°C [32], prior to imaging of MB cell migration within this precise biochemical environment; therefore, all data is collected within steady-state

concentration gradient fields for 24 hours. Our group has previously showed that MB cells migrate and proliferate *in-vitro* until 72 hours in the μLane system [14].

Statistics

One-way ANOVA and Post Hoc Test (Tukey) were used to analyze the data using IBM SPSS Statistics Program (IBM Corp., Released 2011, version 20.0. Armonk, NY). A one-way ANOVA test at a 95% confidence interval was performed for statistical significance across growth factors. The Post Hoc Test (Tukey) was performed to determine the disparity among different groups. Only p-values <0.05 were considered statistically significant. Unpaired student's t-test at a 95% confidence interval was implemented to determine significance of relative receptor expression using IBM SPSS Statistics Program (IBM Corp., Released 2011, version 20.0. Armonk, NY).

Imaging and Processing

Transmitted light microscopy images were obtained using an inverted microscope (Nikon TE2000) and a cooled CCD camera (CoolSNAP EZ CCD Camera, Photometrics, Tucson, AZ) with a 20X objective magnification (Nikon Plant 20X, Morrell Instrument Company Inc., Melville, NY). Fluorescent imaging was performed using Leica CLSM confocal microscope and a Zeiss LSM 710 confocal microscope, both at 63x magnification with oil immersion objective. Image J was utilized to track cells and process images (Chemotaxis and Migration Tool plugin (ImageJ 1.46r) [14, 15]. Fluorescence intensity was measured using an average over the entire cell area via ImageJ. Transmitted light image data was analyzed using Nikon software (Nikon Instrument Element 2.30 with 6D module, Morrell Instrument Company Inc., Melville, NY) and ImageJ (NIH) Software. Bright field images of the microchannel were automatically captured every hour for 24 hours at every 1000 microns in the y-direction of the μLane, followed by cell tracking (n_{cells}~180 cells) and analysis. Lastly, the cell tracking software was used to develop Wind-Rose plots [33, 69] of cell trajectories in response to EGF and SDF-1 gradient fields, over 24 hours.

RESULTS

This work examined the migratory and cellular responses of MB-derived cells in response to external signaling from EGF, HGF, PDGF-BB, and SDF-1.

Motility Studies

The first set of experiments measured the average numbers of MB-derived cells that migrated toward different concentrations of EGF, HGF, PDGF-BB, and SDF-1 through transmembrane assays, as illustrated in Figure 1 and Table 1. As seen, numbers of motile cells were statistically different in response to signaling from different concentrations of EGF and HGF when compared to controls (i.e. no ligand). Further, a mid-level concentration of 100-ng/mL of EGF was observed to attract the largest numbers of motile cells overall (Fig. 1.B.2). By contrast, the number of MB cells that migrated in response to external signaling from concentrations of SDF-1 did not exhibit statistical difference from controls or each other (Fig. 1.B.4). Similarly, the number of motile MB in response to

signaling from different concentrations of PDGF-BB did not display statistical differences from controls (Fig. 1.B.3).

Relative Receptor Expression

The basal expression levels of the respective receptors were then compared against their activation levels upon ligand stimulation. Confocal images in Figure 2 illustrate differences in cellular distribution of activated receptors, as well as differences in fluorescent intensity after ligand stimulation. As seen, basal receptor expression appears to be uniformly distributed throughout the cell cytosol, with lowest intensities measured for EGF-R. Upon ligand activation, receptor expression is increased, but remains largely distributed throughout the cytosol. However, EGF-R expression is also observed to be acutely concentrated along the outer cell membrane. Analysis of fluorescence intensity then represented relative receptor expression levels upon ligand-stimulation. MB stimulated with EGF exhibited the highest increase in receptor expression for EGF-R, with a 3.5-fold increase in intensity over basal EGF-R expression measured in unstimulated controls (Fig. 2.A). By contrast, the expression of CXCR4, the receptor for SDF-1, was approximately 2-fold higher than its basal intensity levels in cells unstimulated with ligand (Fig. 2.B), while no statistical difference was measured between the activation levels of c-Met, the receptor for HGF (Fig. 2.C), and control cells, as well as between PDGFR-BB (Fig 2.D) in ligand-stimulated cells compared to controls. MB cells stimulated with EGF for different time points of 0, 14, 22, 36, and 42 hours displayed no relevant significant difference in receptor expression for EGF-R across time points, and were all higher than the unstimulated control (See supplementary Figure 1).

Migratory response to controlled concentration and gradient fields

The migratory behavior of MB was next examined using our microfluidic system, called the μLane and shown in Figure 3, for real-time cell imaging and analysis. The transport of EGF and SDF-1 along the μLane was modeled computationally, and verified experimentally as previously reported by our group [32]. The system produced a range of concentration gradients along the microchannel length at steady-state, as shown in Figure 4.A [14, 33]. Concentration gradients of this study are defined as the average difference in growth factor concentration (ng/mL) along the microchannel length (mm). Five orders of concentration gradient, G_1-G_5, were delineated along the microchannel as illustrated in Figure 4.A: $10^{+1}<G_1<10^{0}$ ng/(mL.mm), $10^{0}<G_2<10^{-1}$ ng/(mL.mm), $10^{-1}<G_3<10^{-2}$ ng/(mL.mm), $10^{-2}<G_4<10^{-3}$ ng/(mL.mm), and $10^{-3}<G_5<0$. The lowest gradient, G_5, was located near the source reservoir (growth factors only) and occupied approximately 1-mm-length of the microchannel, while the highest gradient, G_1, was located near the sink reservoir and occupied an approximate, 3-mm-length of microchannel. Concentration gradients, G_2, G_3, and G_4, occupied the remaining 9-mm-length of microchannel (distance in between the source and the sink reservoirs) with approximately 4 mm, 3 mm and 2 mm segments, respectively. Note, the core distributions of EGF and SDF-1 along the microchannel are very similar to one another given their respective molecular weights of 6.045 KDa and 7.9 KDa, and hence only one representative gradient distribution is shown. Further, cells were evenly distributed along all segments of the channel prior to the start of experiments.

The migration of MB-derived cells in response to the different concentration gradient fields of EGF and SDF-1 were described using three parameters: (1) Fraction of motile cells, **f,** defined as the number of cells that migrated more than two cell diameters in the*μ*Lane, normalized by the total number of cells within the channel; (2) cell directionality**, D,** defined as the percentage of cells whose net center of mass was preferably towards the positive, x-displacement or along the gradient direction; and (3) Average cell path length, **PL**, defined as the total distance traveled by cells.

First, the average percentage of motile cells along the entire microchannel was similar for both growth factors. Table 2 shows that 72.82% of MB became motile in response to EGF signaling, while an average 67.3% of MB became motile in response to SDF-1 concentration fields. Values of motile fraction varied with gradient fields, $\mathbf{f}^{G1}$-$\mathbf{f}^{G5}$, for both EGF and SDF-1, as shown in Table 3. As seen, the highest fraction of MB cells became motile when exposed to higher concentration gradient fields of EGF, G_1 (f1=28.3%) and G_2 (f2=18.6%), followed by decreasing percentages of motile cells within lower gradient fields of EGF, G_3 (f3=11.9%), G_4 (f4=10.3%) and G_5 (f5=3.7%). Similarly decreasing fractions of cells were seen to migrate in response to concentration gradient fields of SDF-1, with highest fractions at G_1 (f1=18.2%) and G_2 (f2=20%), followed by significant decreases in the fraction of motile cells at concentration gradient fields G_3 (f3=13.8%), G_4 (f4=8.7%) and G_5 (f5=6.5%). As shown in Figure 4.B, the fraction of nonmotile cells was 27.2% and 32.8%, when exposed to similar concentration gradients of EGF and SDF-1, respectively. Statistical significance was observed between concentration gradient fields of EGF while no statistical significant difference was found across the gradient fields of SDF-1.

Next, the average directionality of motile MB was determined by examining individual cell trajectories. The term directionality was previously introduced by our group as the ratio of the number of cells whose centroids migrated more than 80 μm to the total number of cells in the microchannel [(33)]. The paths of MB cells in the presence of EGF and SDF-1 concentration gradient fields were optically tracked within the *μ*Lane system to generate the representative Wind-Rose plots shown in Figure 5.A. Note that although cell trajectories are each positioned at a common origin for comparison, cell paths were measured along all microchannel segments, exposed to all gradient fields G_1-G_5. Representative trajectories illustrate that cells migrated preferentially towards lower concentration gradients of EGF (i.e., towards the right). By contrast, SDF-1 fields resulted in MB migration that was both towards and away from lower SDF gradients without preference. The directionality of motile cells along the entire microchannel was higher for cells stimulated with EGF (61.6%) than SDF-1 (44.2%), shown in Table 2. As seen, cell directionality within specific gradient fields, D^{G1}-D^{G5}, decreased with decreasing gradient for both EGF and SDF-1, shown in Table 3. EGF D^{G1} indicates that 28.3% of motile cells migrated directionally when exposed to G_1 of EGF (i.e. within the first 3mm of channel length), while SDF D^{G1} denotes that only 18.4% displayed directional migration for the same gradient field of SDF-1. The highest fraction of MB cells directionality was reported at higher concentration gradient fields of EGF, D^{G1} (28.3%) and D^{G2} (15%), followed by decreasing percentages for directionality within lower gradient fields of EGF, D^{G3} (7%), D^{G4} (8.6%), and D^{G5} (2.7%). Similarly decreasing fractions of directionality were reported in response to concentration gradient

fields of SDF-1, with highest fractions at D^{G1} (18.4%) and D^{G2} (10.5%), followed by decreasing fractions of directionality at D^{G3} (9.8%), D^{G4} (2.2%), and D^{G5} (3.3%).

In addition, Wind-Rose plots display the average maximum cell path length, **PL**, of motile cells tracked along the entire microchannel. Using this data, 32% of motile MB migrated distances greater than 200 microns (or 20 cell-diameters) when exposed to EGF gradient fields, as seen in Figure 5.B. By contrast, 97.3% of cells exposed to SDF-1 gradients migrated distances less than 200 microns. MB within our *μ*Lane system in the absence of growth factors or concentration gradients (i.e. controls) displayed migration distances between 50 and 200 microns [(14)]. As shown, increasing percentages of cells were seen to migrate in response to higher gradient fields of EGF. A larger percentage of motile MB were observed in response to G_1 fields of EGF at every distance, while only cells exposed to G_1 migrated the longest distances greater than 300 microns. In comparison, MB exposed to lower gradient fields of SDF-1 (G_3-G_5) exhibited the longest migration. Notably, zero cells were observed to migrate less than 100 microns when exposed to any EGF gradient field G_1-G_5, while zero cells were seen to migrate greater than 300 microns when exposed to any SDF-1 gradient fields G_1-G_5.

DISCUSSION

The chemotactic migration of MB-derived cells has been surprisingly understudied despite its well-known metastatic potential and aggressive invasion into the brain and spinal cord [(14, 43)]. Our study is among the first to examine and compare the migratory responses of MB to dosage-dependent signaling from EGF, HGF, PDGF-BB, and SDF-1, the most widely-acknowledged chemoattractants of CNS tumor cells [(37)]. The first set of experiments utilized conventional transwell assays to illustrate that MB migration was most concentration-dependent to EGF signaling. As shown in Figure 1, MB exhibited dosage-dependent migration in response to signaling from EGF and HGF, but seemingly dosage-independent responses to PDGF and SDF-1 signaling. Further, EGF simulated the migration of approximately twice the number of MB cells than did PDGF, HGF, or SDF-1. Results from immunocytochemistry support the strength of MB chemotactic response to EGF signaling, as activation of its receptor, EGF-R, was two times larger than activation of other respective receptors. While strong MB chemotactic response to EGF signaling is consistent with previous findings from our group and others [(14, 42)], it is most significant here because it is signaling from SDF-1, rather than EGF, that has been reported as the strongest MB chemoattractant [(56)]. Inhibitor AMD310, which cleaves CXCR4, has been reported to decrease MB tumor growth in mouse xenografts, chemotaxis and proliferation [(56)]. However, *in vivo* use of EGF-R inhibitors such as Tarceva and Gefitinib have reported no changes in motility of cells derived from glioma [(47)], and non-small-cell lung cancer [(23)], and thus, were minimally used on MB. We contend that MB chemotactic response may not have been measured most meaningfully in the past, which has stymied development of anti-migratory therapies for MB metastasis. For this reason, we used microfluidic systems to more precisely study MB migratory responses using parameters relevant to metastasis.

Using the *μ*Lane system, we were able to image real-time cell behavior in response to a wide range of concentrations and gradients of EGF and SDF-1, and distinguish directed-migration

of chemotaxis. MB migratory behavior was observed to be concentration gradient-dependent for both EGF and SDF-1 signaling, as the fraction of motile cells decreased with decreasing concentration gradient in both cases. However, motile MB traveled longer distances within the *μ*Lane in response to EGF signaling, with an average PL of 264.5 ± 67.8 μm, compared to an average PL of 125.5 ± 48.6 μm when responding to signaling from SDF-1. Further, cell trajectories illustrated an MB directional bias towards decreasing EGF gradients not present with SDF-1 signaling, with 18.3% of cells migrating towards decreasing EGF gradients compared to 15.3% of MB in response to decreasing SDF-1 gradients. Importantly, this behavior was observed along the entire *μ*Lane length, for cells exposed to all concentration gradient fields, $G_{1\text{-}5}$. Here, the cell directionality compared to other methods provides insight into whether MB cells stimulated with ligand solutions (EGF or SDF-1) followed a directional migration along gradient fields. Other methods to measure cell migration include the persistence length and average velocity to determine the chemotactic sensitivity of stable gradients in 3D [22, 46, 72, 75]. While the persistence length provides the ratio of the net distance traveled to the total distance, it would not report the number of cells that migrate along ligand concentration gradients, which is highly significant to studies developing migration-targeted therapies for tumors of the CNS.

This consistent MB behavior illustrates that EGF signaling from high concentration gradients initiates the most motile MB, and further enables cells to travel the longest distances. MB cells were seen to migrate towards increasing ligand concentration, which also corresponds to decreasing EGF gradient fields in our system. This response is significant because it reflects MB sensitivity to high concentration gradients (G_1-G_2), which were generated via much greater nonlinear changes in ligand concentration as compared to low gradient fields (G_3-G_5). Previous work from our group has illustrated keen abilities of MB to migrate in larger numbers in response to increasing EGF concentration via pERK signaling [14]. In that work, MB cells were seen to travel out of a cell reservoir when exposed to increasing gradients and concentration. In the current study, we now demonstrate that MB can become less motile when exposed to signaling from increasing concentration but diminishing EGF gradient fields.

Data from the current study highlights the high fraction of motile MB in response to high concentration gradients of EGF. These results have high clinical interpretation, as they point to high gradient fields and low concentration fields as optimal for MB migration. This is an *in-vivo* scenario where paracrine signaling from neighboring cells initiate the most MB migration, such that cell displacement diminishes as cells approach the signaling source, where gradients are low and concentration is high. In addition, our findings may aid clinical development of anti-migratory therapeutics with the potential to inhibit MB metastasis along the spinal column via EGF signaling.

CONCLUSION

In summary, our results illustrate that MB migration is both concentration and concentration gradient-dependent in response to EGF signaling. Further, our findings illustrate that high gradient fields of EGF result in the largest number of motile cells, which travel long

distances, and in a highly directional manner towards decreasing EGF gradients. These findings point to EGF as a viable molecule for migration-targeted therapies for MB.

Supplementary Material

Refer to Web version on PubMed Central for supplementary material.

ACKNOWLEDGEMENTS

This has been supported by NIH CA 118255 and NSF CBET 09395117. The authors wish to thank Mr. Uchenna Unachukwu and Mr. Shawn Mishra for their technical assistance in this work.

REFERENCES

1. Able, R.; Dudu, V.; Vazquez, M. Migration and Invasion of Brain Tumors. InTech; Croatia: 2011. p. 225-256.
2. Able RA Jr. Ngnabeuye C, Beck C, Holland EC, Vazquez M. Low Concentration Microenvironments Enhance the Migration of Neonatal Cells of Glial Lineage. Cell Mol Bioeng. 5:2012.
3. Abouantoun TJ, Castellino RC, MacDonald TJ. Sunitinib induces PTEN expression and inhibits PDGFR signaling and migration of medulloblastoma cells. J Neurooncol. 2011; 101:215–226. [PubMed: 20524040]
4. Abouantoun TJ, MacDonald TJ. Imatinib blocks migration and invasion of medulloblastoma cells by concurrently inhibiting activation of platelet-derived growth factor receptor and transactivation of epidermal growth factor receptor. Mol Cancer Ther. 2009; 8:1137–1147. [PubMed: 19417143]
5. Algaidi SA, Christie LA, Jenkinson AM, Whalley L, Riedel G, Platt B. Long-term homocysteine exposure induces alterations in spatial learning, hippocampal signalling and synaptic plasticity. Experimental neurology. 2006; 197:8–21. [PubMed: 16095594]
6. Barnwell SL, Edwards MS. Spinal intramedullary spread of medulloblastoma. Case report. J Neurosurg. 1986; 65:253–255. [PubMed: 3723185]
7. Carlotti CG Jr. Smith C, Rutka JT. The molecular genetics of medulloblastoma: an assessment of new therapeutic targets. Neurosurg Rev. 2008; 31:359–368. discussion 368-359. [PubMed: 18548301]
8. Charles NA, Holland EC, Gilbertson R, Glass R, Kettenmann H. The brain tumor microenvironment. Glia. 2012; 60:502–514. [PubMed: 22379614]
9. Condeelis J, Segall JE. Intravital imaging of cell movement in tumours. Nat Rev Cancer. 2003; 3:921–930. [PubMed: 14737122]
10. Cselenyi Z, Farde L. Quantification of blood flow-dependent component in estimates of beta-amyloid load obtained using quasi-steady-state standardized uptake value ratio. Journal of cerebral blood flow and metabolism : official journal of the International Society of Cerebral Blood Flow and Metabolism. 2015
11. Curry FE. Determinants of capillary permeability: a review of mechanisms based on single capillary studies in the frog. Circ Res. 1986; 59:367–380. [PubMed: 3791580]
12. Curry FR. The Eugene M. Landis Award Lecture. 1993. Regulation of water and solute exchange in microvessel endothelium; studies in single perfused capillaries. Microcirculation. 1994; 1:11–26. [PubMed: 8790574]
13. Dhall G. Medulloblastoma. J Child Neurol. 2009; 24:1418–1430. [PubMed: 19841429]
14. Dudu V, Able RA Jr. Rotari V, Kong Q, Vazquez M. Role of Epidermal Growth Factor-Triggered PI3K/Akt Signaling in the Migration of Medulloblastoma-Derived Cells. Cell Mol Bioeng. 2012; 5:502–413. [PubMed: 24273611]
15. Dudu V, Rotari V, Vazquez M. Targeted extracellular nanoparticles enable intracellular detection of activated epidermal growth factor receptor in living brain cancer cells. Nanomedicine. 2011; 7:896–903. [PubMed: 21683807]

16. Duffner PK, Horowitz ME, Krischer JP, Burger PC, Cohen ME, Sanford RA, Friedman HS, Kun LE. The treatment of malignant brain tumors in infants and very young children: an update of the Pediatric Oncology Group experience. Neuro Oncol. 1999; 1:152–161. [PubMed: 11554387]
17. Ellina MI, Bouris P, Aletras AJ, Theocharis AD, Kletsas D, Karamanos NK. EGFR and HER2 exert distinct roles on colon cancer cell functional properties and expression of matrix macromolecules. Biochim Biophys Acta. 2014; 1840:2651–2661. [PubMed: 24792576]
18. Ferguson SJ, Ito K, Nolte LP. Fluid flow and convective transport of solutes within the intervertebral disc. J Biomech. 2004; 37:213–221. [PubMed: 14706324]
19. Fomchenko EI, Holland EC. Stem cells and brain cancer. Exp Cell Res. 2005; 306:323–329. [PubMed: 15925587]
20. Fu B, Curry FR, Adamson RH, Weinbaum S. A model for interpreting the tracer labeling of interendothelial clefts. Ann Biomed Eng. 1997; 25:375–397. [PubMed: 9084841]
21. Gerber NU, Mynarek M, von Hoff K, Friedrich C, Resch A, Rutkowski S. Recent developments and current concepts in medulloblastoma. Cancer Treat Rev. 2014; 40:356–365. [PubMed: 24389035]
22. Haessler U, Pisano M, Wu M, Swartz MA. Dendritic cell chemotaxis in 3D under defined chemokine gradients reveals differential response to ligands CCL21 and CCL19. Proc Natl Acad Sci U S A. 2011; 108:5614–5619. [PubMed: 21422278]
23. Heon S, Yeap BY, Lindeman NI, Joshi VA, Butaney M, Britt GJ, Costa DB, Rabin MS, Jackman DM, Johnson BE. The impact of initial gefitinib or erlotinib versus chemotherapy on central nervous system progression in advanced non-small cell lung cancer with EGFR mutations. Clinical cancer research : an official journal of the American Association for Cancer Research. 2012; 18:4406–4414. [PubMed: 22733536]
24. Hoang DH, Pagnier A, Guichardet K, Dubois-Teklali F, Schiff I, Lyard G, Cousin E, Krainik A. Cognitive disorders in pediatric medulloblastoma: what neuroimaging has to offer. J Neurosurg Pediatr. 2014:1–9.
25. Huang Y, Rumschitzki D, Chien S, Weinbaum S. A fiber matrix model for the growth of macromolecular leakage spots in the arterial intima. Journal of biomechanical engineering. 1994; 116:430–445. [PubMed: 7869719]
26. Irimia D. Microfluidic technologies for temporal perturbations of chemotaxis. Annual review of biomedical engineering. 2010; 12:259–284.
27. Keenan TM, Folch A. Biomolecular gradients in cell culture systems. Lab on a chip. 2008; 8:34–57. [PubMed: 18094760]
28. Khatua S, Zaky W. The biologic era of childhood medulloblastoma and clues to novel therapies. Future Oncol. 2014; 10:637–645. [PubMed: 24754593]
29. Kim S, Kim HJ, Jeon NL. Biological applications of microfluidic gradient devices. Integrative biology : quantitative biosciences from nano to macro. 2010; 2:584–603. [PubMed: 20957276]
30. Kim WS, Tarbell JM. Macromolecular transport through the deformable porous media of an artery wall. Journal of biomechanical engineering. 1994; 116:156–163. [PubMed: 8078322]
31. Kinsey ST, Moerland TS. Metabolite diffusion in giant muscle fibers of the spiny lobster Panulirus argus. J Exp Biol. 2002; 205:3377–3386. [PubMed: 12324547]
32. Kong Q, Able RA Jr. Dudu V, Vazquez M. A microfluidic device to establish concentration gradients using reagent density differences. Journal of biomechanical engineering. 2010; 132:121012. [PubMed: 21142326]
33. Kong Q, Majeska RJ, Vazquez M. Migration of connective tissue-derived cells is mediated by ultra-low concentration gradient fields of EGF. Exp Cell Res. 2011; 317:1491–1502. [PubMed: 21536028]
34. Lauffenburger DA, Horwitz AF. Cell migration: a physically integrated molecular process. Cell. 1996; 84:359–369. [PubMed: 8608589]
35. Lauritzen HP, Ploug T, Prats C, Tavare JM, Galbo H. Imaging of insulin signaling in skeletal muscle of living mice shows major role of T-tubules. Diabetes. 2006; 55:1300–1306. [PubMed: 16644686]
36. Liang CC, Park AY, Guan JL. In vitro scratch assay: a convenient and inexpensive method for analysis of cell migration in vitro. Nature protocols. 2007; 2:329–333. [PubMed: 17406593]

37. Logan A. CNS growth factors. British journal of hospital medicine. 1990; 43:428–437. [PubMed: 2194623]
38. Louis DN, Ohgaki H, Wiestler OD, Cavenee WK, Burger PC, Jouvet A, Scheithauer BW, Kleihues P. The 2007 WHO classification of tumours of the central nervous system. Acta Neuropathol. 2007; 114:97–109. [PubMed: 17618441]
39. Lutostansky EM, Karner G, Rappitsch G, Ku DN, Perktold K. Analysis of hemodynamic fluid phase mass transport in a separated flow region. Journal of biomechanical engineering. 2003; 125:189–196. [PubMed: 12751280]
40. Matthaeus WH, Wan M, Servidio S, Greco A, Osman KT, Oughton S, Dmitruk P. Intermittency, nonlinear dynamics and dissipation in the solar wind and astrophysical plasmas. Philosophical transactions Series A, Mathematical, physical, and engineering sciences. 373:2015.
41. Mohanty CB, Shukla DP, Devi BI. Brain tumors of infancy - an institutional experience and review of the literature. Pediatr Neurosurg. 2013; 49:145–154. [PubMed: 24662246]
42. Mosadegh B, Saadi W, Wang SJ, Jeon NL. Epidermal growth factor promotes breast cancer cell chemotaxis in CXCL12 gradients. Biotechnol Bioeng. 2008; 100:1205–1213. [PubMed: 18553401]
43. Northcott PA, Korshunov A, Pfister SM, Taylor MD. The clinical implications of medulloblastoma subgroups. Nat Rev Neurol. 2012; 8:340–351. [PubMed: 22565209]
44. Packer RJ, Zhou T, Holmes E, Vezina G, Gajjar A. Survival and secondary tumors in children with medulloblastoma receiving radiotherapy and adjuvant chemotherapy: results of Children's Oncology Group trial A9961. Neuro Oncol. 2013; 15:97–103. [PubMed: 23099653]
45. Papadopoulos S, Jurgens KD, Gros G. Protein diffusion in living skeletal muscle fibers: dependence on protein size, fiber type, and contraction. Biophys J. 2000; 79:2084–2094. [PubMed: 11023912]
46. Petrie RJ, Doyle AD, Yamada KM. Random versus directionally persistent cell migration. Nat Rev Mol Cell Biol. 2009; 10:538–549. [PubMed: 19603038]
47. Pfeffer MR, Levitt ML, Aderka D. Gefitinib in recurrent glioblastoma. Journal of clinical oncology : official journal of the American Society of Clinical Oncology. 2004; 22:2755–2756. author reply 2756. [PubMed: 15226353]
48. Pilkington GJ, Bjerkvig R, De Ridder L, Kaaijk P. In vitro and in vivo models for the study of brain tumour invasion. Anticancer research. 1997; 17:4107–4109. [PubMed: 9428342]
49. Provencal M, Labbe D, Veitch R, Boivin D, Rivard GE, Sartelet H, Robitaille Y, Gingras D, Beliveau R. c-Met activation in medulloblastoma induces tissue factor expression and activity: effects on cell migration. Carcinogenesis. 2009; 30:1089–1096. [PubMed: 19359592]
50. Ranger A, McDonald W, Bauman GS, Del Maestro R. Effects of surgical excision and radiation on medulloblastoma cell invasiveness. Can J Neurol Sci. 2009; 36:631–637. [PubMed: 19831134]
51. Ray GL, Buchsbaum JC, McMullen KP, Simoneaux RV, Hines M, Douglas JG, Johnstone PA. Definitive treatment of leptomeningeal spinal metastases in children. Pediatr Blood Cancer. 2013; 60:1839–1841. [PubMed: 23788317]
52. Reddy AT. Advances in biology and treatment of childhood brain tumors. Curr Neurol Neurosci Rep. 2001; 1:137–143. [PubMed: 11898509]
53. Rieken S, Rieber J, Brons S, Habermehl D, Rief H, Orschiedt L, Lindel K, Weber KJ, Debus J, Combs SE. Radiation-induced motility alterations in medulloblastoma cells. J Radiat Res. 2015
54. Rodriguez LG, Wu X, Guan JL. Wound-healing assay. Methods in molecular biology. 2005; 294:23–29. [PubMed: 15576902]
55. Ronning C, Sundet K, Due-Tonnessen B, Lundar T, Helseth E. Persistent cognitive dysfunction secondary to cerebellar injury in patients treated for posterior fossa tumors in childhood. Pediatr Neurosurg. 2005; 41:15–21. [PubMed: 15886508]
56. Rubin JB, Kung AL, Klein RS, Chan JA, Sun Y, Schmidt K, Kieran MW, Luster AD, Segal RA. A small-molecule antagonist of CXCR4 inhibits intracranial growth of primary brain tumors. Proc Natl Acad Sci U S A. 2003; 100:13513–13518. [PubMed: 14595012]
57. Saadi W, Wang SJ, Lin F, Jeon NL. A parallel-gradient microfluidic chamber for quantitative analysis of breast cancer cell chemotaxis. Biomed Microdevices. 2006; 8:109–118. [PubMed: 16688570]

58. Sahai E. Mechanisms of cancer cell invasion. Curr Opin Genet Dev. 2005; 15:87–96. [PubMed: 15661538]
59. Salsman VS, Chow KK, Shaffer DR, Kadikoy H, Li XN, Gerken C, Perlaky L, Metelitsa LS, Gao X, Bhattacharjee M, Hirschi K, Heslop HE, Gottschalk S, Ahmed N. Crosstalk between medulloblastoma cells and endothelium triggers a strong chemotactic signal recruiting T lymphocytes to the tumor microenvironment. PloS one. 2011; 6:e20267. [PubMed: 21647415]
60. Singh T, Kothapalli C, Varma D, Nicoll SB, Vazquez M. Carboxymethylcellulose hydrogels support central nervous system-derived tumor-cell chemotactic migration: Comparison with conventional extracellular matrix macromolecules. J Biomater. Appl;2014
61. Sinzig M, Gasser J, Jauk B, Hausegger KA. [Brain tumors in childhood]. Radiologe. 2008; 48:946–954. [PubMed: 18493733]
62. Soukane DM, Shirazi-Adl A, Urban JP. Analysis of nonlinear coupled diffusion of oxygen and lactic acid in intervertebral discs. Journal of biomechanical engineering. 2005; 127:1121–1126. [PubMed: 16502654]
63. Soukane DM, Shirazi-Adl A, Urban JP. Computation of coupled diffusion of oxygen, glucose and lactic acid in an intervertebral disc. J Biomech. 2007; 40:2645–2654. [PubMed: 17336990]
64. Stefonek-Puccinelli TJ, Masters KS. Regulation of cell signaling and function via changes in growth factor presentation. Conf Proc IEEE Eng Med Biol Soc. 2009; 2009:1167–1171. [PubMed: 19963489]
65. Sumer-Turanligil NC, Cetin EO, Uyanikgil Y. A contemporary review of molecular candidates for the development and treatment of childhood medulloblastoma. Childs Nerv Syst. 2013; 29:381–388. [PubMed: 23292496]
66. Tada S, Tarbell JM. Fenestral pore size in the internal elastic lamina affects transmural flow distribution in the artery wall. Ann Biomed Eng. 2001; 29:456–466. [PubMed: 11459339]
67. Tripathi M, Jain N, Jaimini A, Garg G, D'Souza M M, Sharma R, Grover RK, Mondal A. Demonstration of diffuse leptomeningeal metastasis in a treated case of medulloblastoma with F-18 FDG PET/CT. Clin Nucl Med. 2009; 34:530–532. [PubMed: 19617737]
68. Tzeghai G, Weinbaum S, Pfeffer R. A steady-state filtration model for transluminal water movement in small and large blood vessels. Journal of biomechanical engineering. 1985; 107:123–130. [PubMed: 3999708]
69. Unachukwu UJ, Sauane M, Vazquez M, Redenti S. Microfluidic generated EGF-gradients induce chemokinesis of transplantable retinal progenitor cells via the JAK/STAT and PI3kinase signaling pathways. PLoS One. 2013; 8:e83906. [PubMed: 24376770]
70. Venkataraman S, Alimova I, Balakrishnan I, Harris P, Birks DK, Griesinger A, Amani V, Cristiano B, Remke M, Taylor MD, Handler M, Foreman NK, Vibhakar R. Inhibition of BRD4 attenuates tumor cell self-renewal and suppresses stem cell signaling in MYC driven medulloblastoma. Oncotarget. 2014; 5:2355–2371. [PubMed: 24796395]
71. Weaver JB, Van Houten EE, Miga MI, Kennedy FE, Paulsen KD. Magnetic resonance elastography using 3D gradient echo measurements of steady-state motion. Medical physics. 2001; 28:1620–1628. [PubMed: 11548931]
72. Weber M, Hauschild R, Schwarz J, Moussion C, de Vries I, Legler DF, Luther SA, Bollenbach T, Sixt M. Interstitial dendritic cell guidance by haptotactic chemokine gradients. Science. 2013; 339:328–332. [PubMed: 23329049]
73. Wen GB, Weinbaum S, Ganatos P, Pfeffer R, Chien S. On the time dependent diffusion of macromolecules through transient open junctions and their subendothelial spread. 2. Long time model for interaction between leakage sites. Journal of theoretical biology. 1988; 135:219–253. [PubMed: 3267768]
74. Wikstrand CJ, Friedman HS, Bigner DD. Medulloblastoma cell-substrate interaction in vitro. Invasion Metastasis. 1991; 11:310–324. [PubMed: 1822845]
75. Wu J, Wu X, Lin F. Recent developments in microfluidics-based chemotaxis studies. Lab Chip. 2013; 13:2484–2499. [PubMed: 23712326]
76. Yamaguchi H, Wyckoff J, Condeelis J. Cell migration in tumors. Curr Opin Cell Biol. 2005; 17:559–564. [PubMed: 16098726]

77. Yang WQ, Senger D, Muzik H, Shi ZQ, Johnson D, Brasher PM, Rewcastle NB, Hamilton M, Rutka J, Wolff J, Wetmore C, Curran T, Lee PW, Forsyth PA. Reovirus prolongs survival and reduces the frequency of spinal and leptomeningeal metastases from medulloblastoma. Cancer Res. 2003; 63:3162–3172. [PubMed: 12810644]

78. Yarrow JC, Perlman ZE, Westwood NJ, Mitchison TJ. A high-throughput cell migration assay using scratch wound healing, a comparison of image-based readout methods. BMC biotechnology. 2004; 4:21. [PubMed: 15357872]

79. Yazigi-Rivard L, Masserot C, Lachenaud J, Diebold-Pressac I, Aprahamian A, Avran D, Doz F. [Childhood medulloblastoma]. Arch Pediatr. 2008; 15:1794–1804. [PubMed: 18995998]

80. Yuan F, Chien S, Weinbaum S. A new view of convective-diffusive transport processes in the arterial intima. Journal of biomechanical engineering. 1991; 113:314–329. [PubMed: 1921359]

81. Zengel P, Nguyen-Hoang A, Schildhammer C, Zantl R, Kahl V, Horn E. mu-Slide Chemotaxis: a new chamber for long-term chemotaxis studies. BMC cell biology. 2011; 12:21. [PubMed: 21592329]

82. Zigmond SH, Hirsch JG. Leukocyte locomotion and chemotaxis. New methods for evaluation, and demonstration of a cell-derived chemotactic factor. J Exp Med. 1973; 137:387–410. [PubMed: 4568301]

83. Zivkovic N, Berisavac I, Markovic M, Milenkovic S. Spinal metastasis of medulloblastoma in adults: a case report. Srp Arh Celok Lek. 2014; 142:713–716. [PubMed: 25731002]

84. Zumpano BJ. Spinal intramedullary metastatic medulloblastoma. Case report. J Neurosurg. 1978; 48:632–635. [PubMed: 632889]

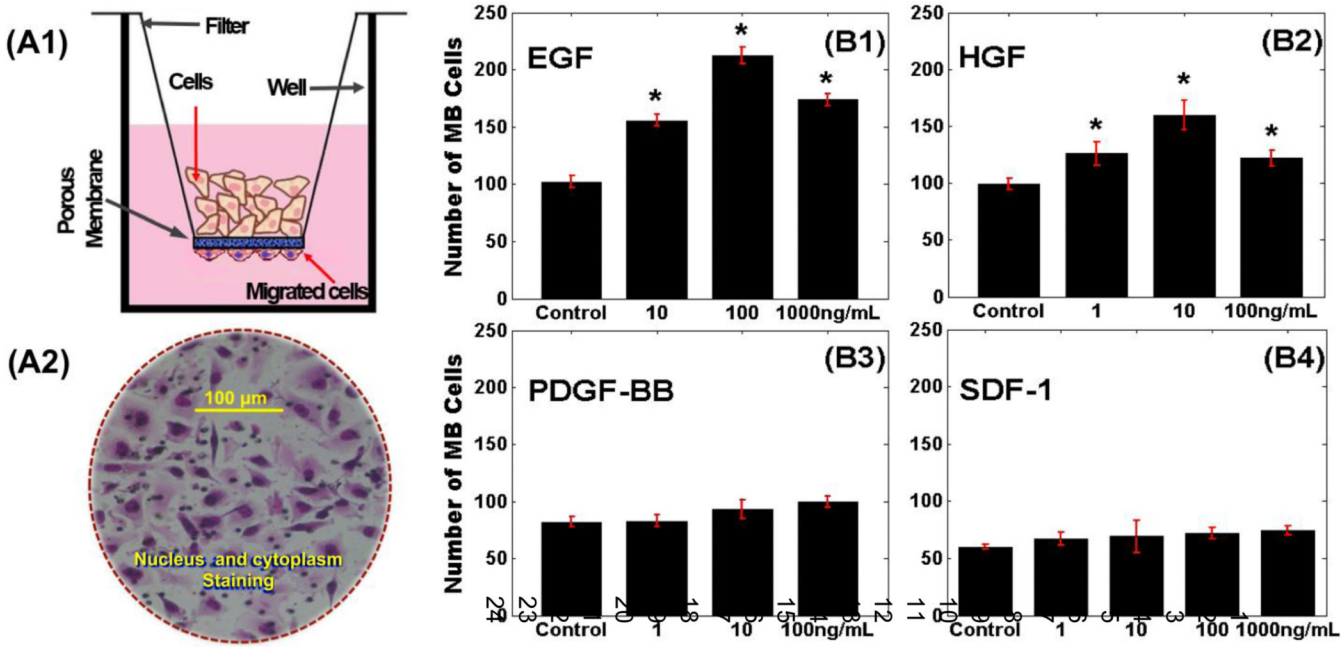

Figure 1. Migration of MB-derived cells to different concentrations of selective chemotactic ligands

(A1) Schematic of transwell assay with motile cells attached to the underside of the porous membrane. (A2) Stained nuclei and cytoplasm of motile MB-derived cells toward different concentrations of (B1) EGF, (B2) HGF, (B3) PDGF, and (B4) SDF-1. The control groups indicate number of cells that migrated towards serum-free medium. An asterisk (*) indicates statistically significant data with p-values <0.05 against control group.

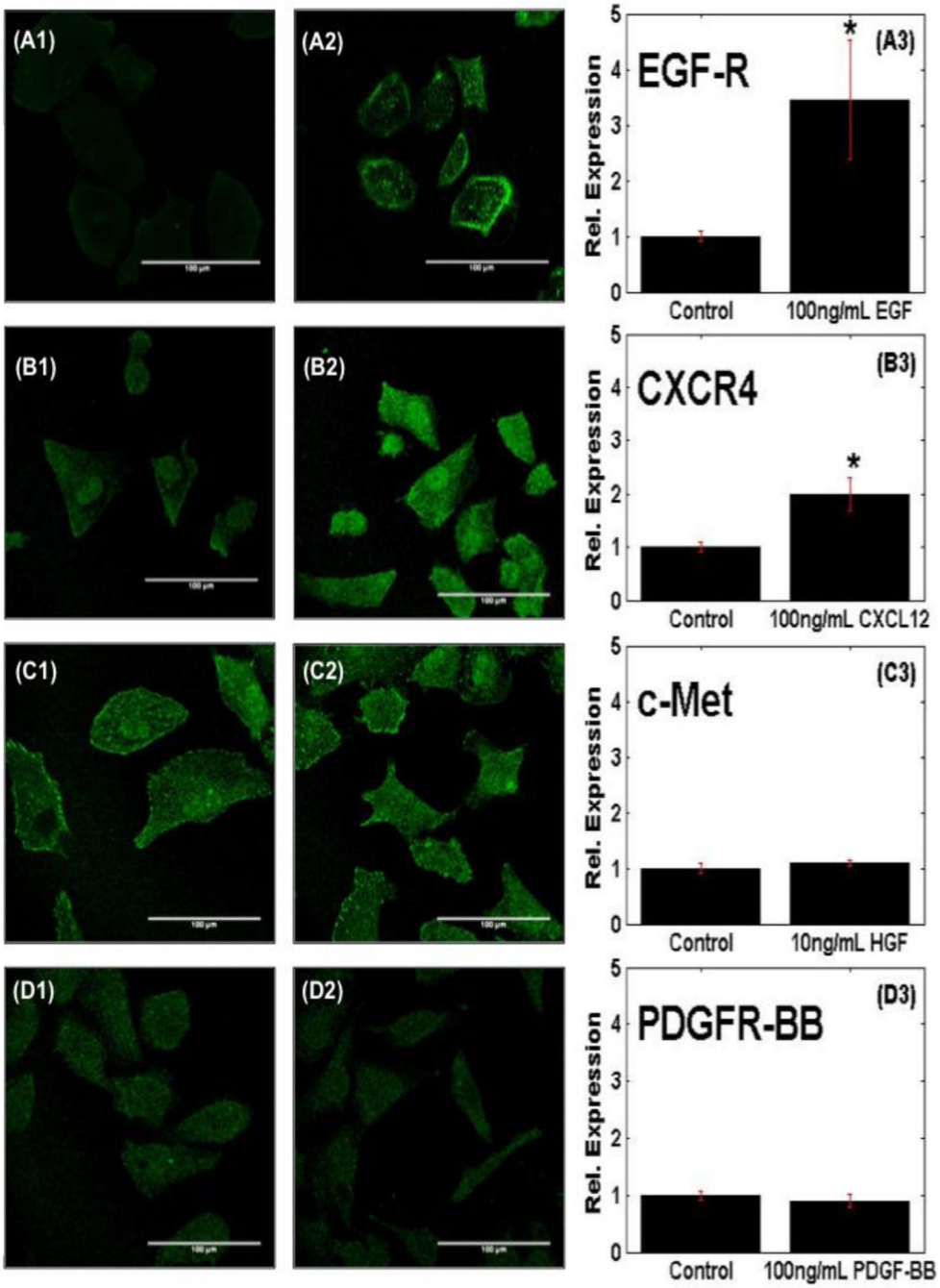

Figure 2. Receptor activation within motile MB-derived cells

Immunocytochemistry of basal receptor expression of MB cells without ligand stimulation to (A1) EGF, (B1) SDF-1, (C1) HGF, and (D1) PDGF-BB. Receptor activation post-stimulation with (A2) EGF, (B2) SDF-1, (C2) HGF, and (D2) PDGF-BB. The expression level of receptor following ligand stimulation of (A3) EGFR, (B3) CXCR4, (C3) c-Met, and (D3) PDGFR-BB normalized to basal control levels. Scale bars are 100μm. An asterisk (*) indicates statistically significant data with p-values <0.05.

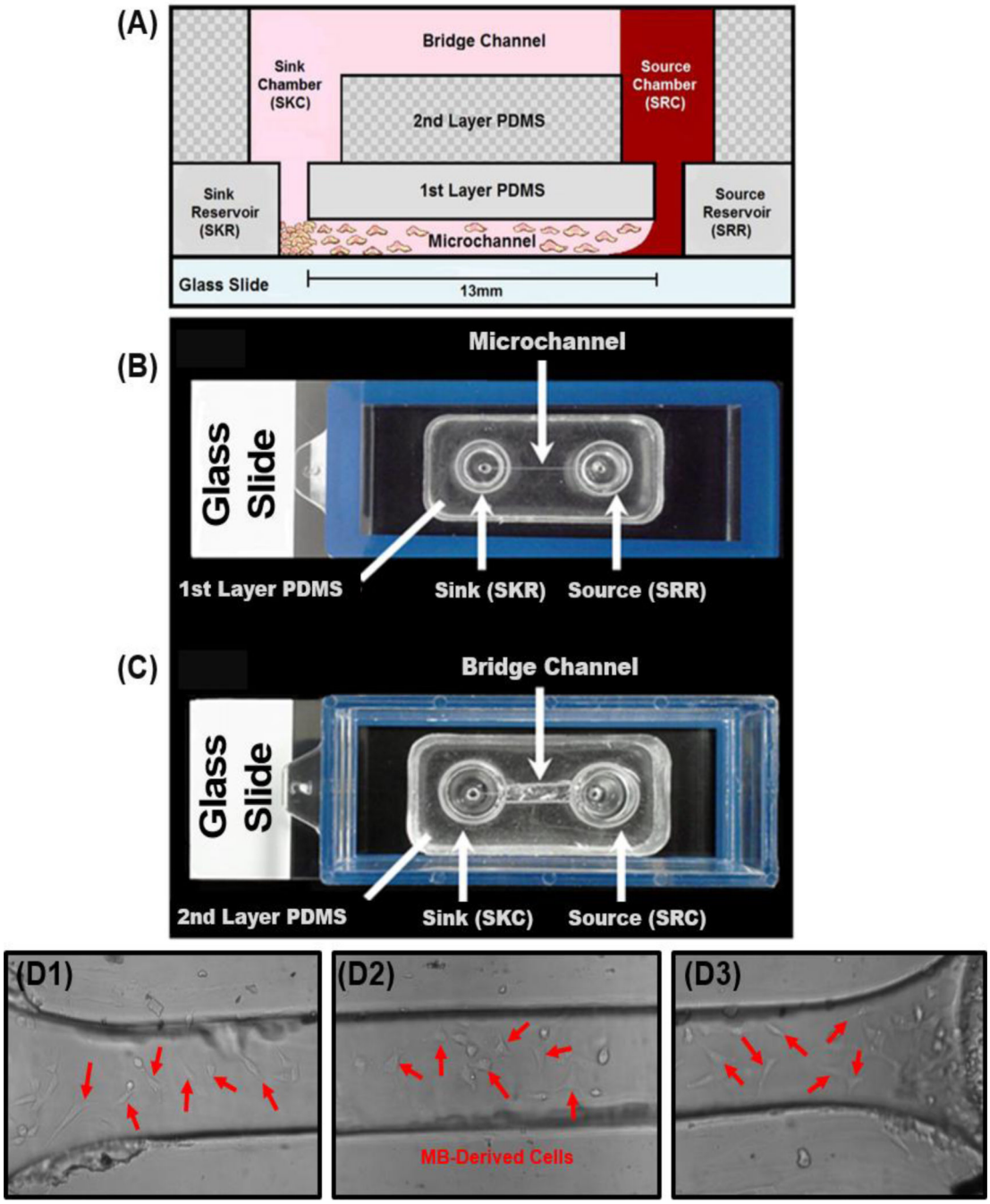

Figure 3. The *μ*Lane system and MB migratory responses

(A) Schematic of the bridged *μ*Lane system, showing cells inserted within the sink (SKR) and source (SRR) reservoir, and adhered along the microchannel. Chemotactic agents (e.g. EGF, SDF-1) are loaded into the source chamber (SRC), and transported to SKR to reach steady-state concentration distribution. (B) Top view image of the first layer PDMS bonded onto a glass slide. Two 9-nL reservoirs are connected by a microchannel of 13mm in length and 100μm in diameter. (C) Top view image of second layer PDMS bonded to the first layer. The source (SRC) and sink (SKC) chambers are connected by a bridge channel. (D)

Raw data image of motile MB cells within μLane system at (D1) source reservoir, (D2) mid channel, and (D3) sink reservoir.

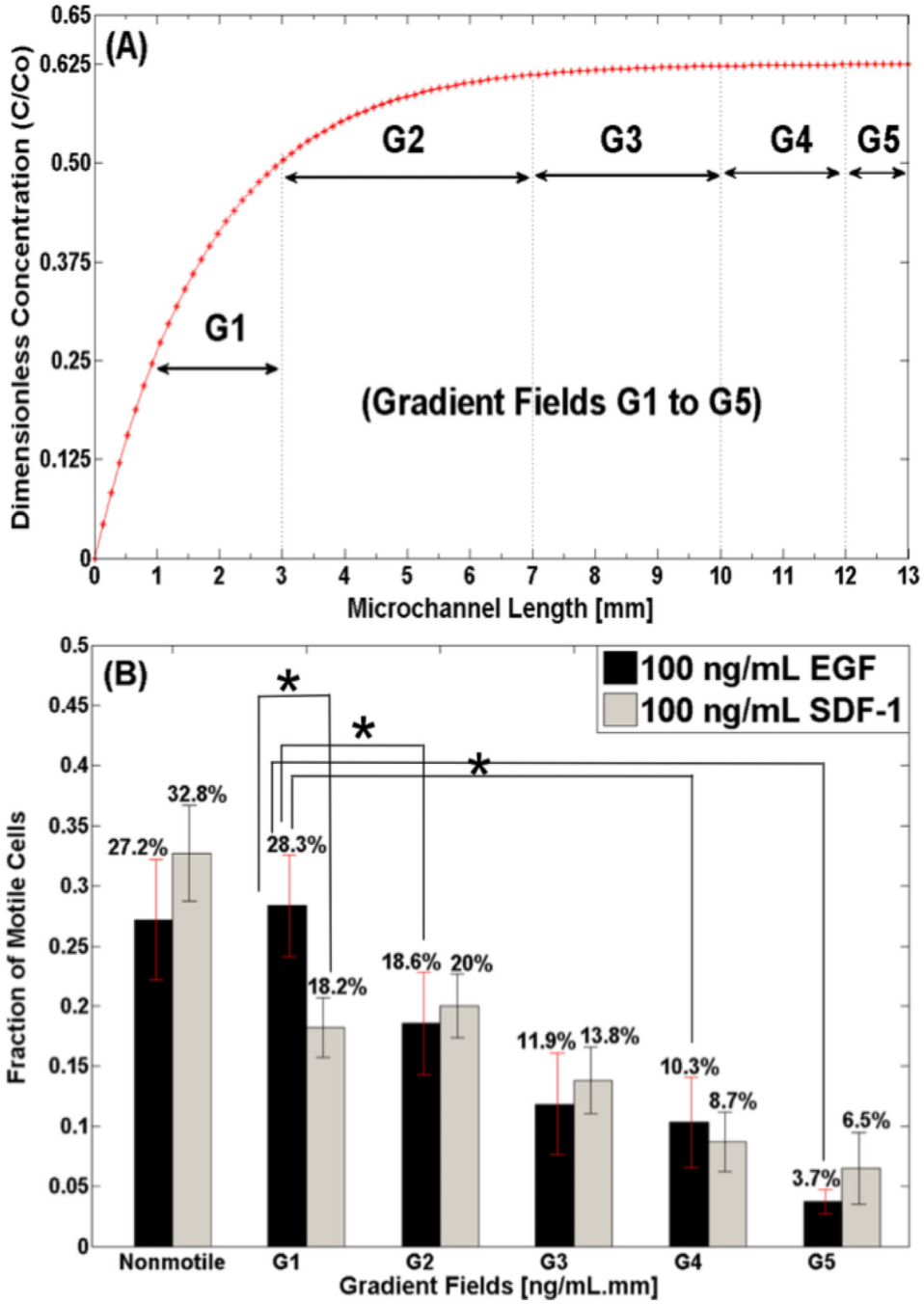

Figure 4. Concentration distribution along *μ*Lane and number of motile cells

(A) Concentration profile of EGF and SDF-1 along 13-mm microchannel length of *μ*Lane system. Concentration gradients are identified by five orders of magnitude in the microchannel: $10^{+1}<G_1<10^{0}$ ng/(mL.mm), $10^{0}<G_2<10^{-1}$ ng/(mL.mm), $10^{-1}<G_3<10^{-2}$ ng/(mL.mm), $10^{-2}<G_4<10^{-3}$ ng/(mL.mm), and $10^{-3}<G_5<0$ ng/(mL.mm). (B) Fraction of MB-derived cells observed to respond via migration to the different concentration gradient fields (G_1 through G_5) of EGF and SDF-1.

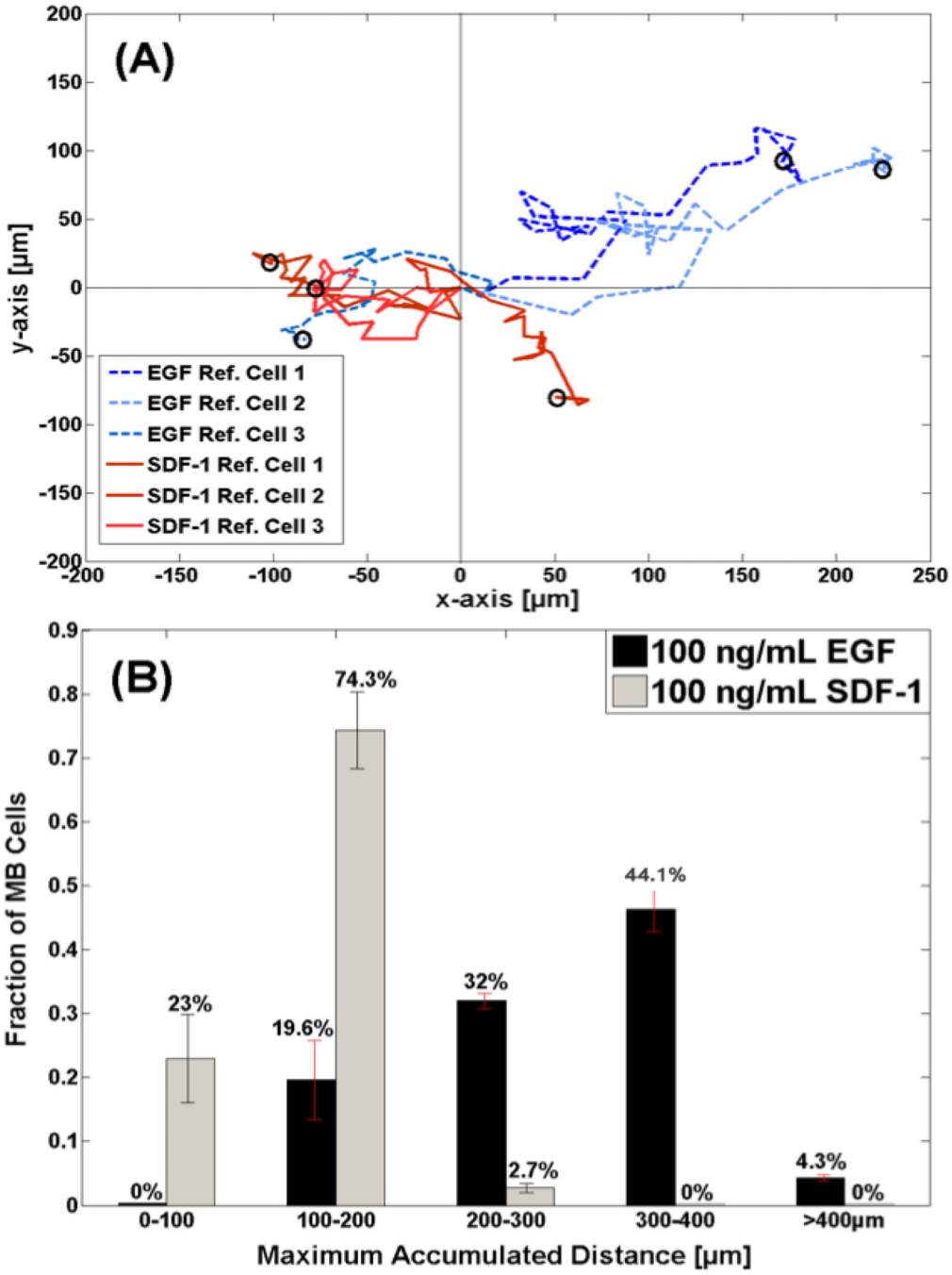

Figure 5. Motility of MB-derived cells in the *μ*Lane system

(A) Representative trajectories of cells that migrated in response to 100ng/mL of EGF and 100 ng/mL of SDF-1 stimulation. Three cell paths are shown in dashed for EGF and three in solid for SDF-1, 24 hours post steady-state. Note that concentration gradients decrease from left to right within the *μ*Lane. (B) Maximum accumulated distance of motile cells stimulated by concentration profiles generated by using 100ng/mL of EGF and 100 ng/mL of SDF-1, respectively, in the SRR of the *μ*Lane.

Table 1

Transwell Results[1].

Growth Factors	0 ng/mL [Mean ± SD cells]	1 ng/mL [Mean ± SD cells]	10 ng/mL [Mean ± SD cells]	100 ng/mL [Mean ± SD cells]	1000 ng/mL [Mean ± SD cells]
EGF	102 ± 5	*	156 ± 5	212 ± 7	174 ± 5
SDF-1	60 ± 2	67 ± 6	69 ± 14	72 ± 5	74 ± 4
HGF	99 ± 5	126 ± 10	160 ±13	122 ± 7	*
PDGF-BB	82 ± 5	83 ± 5	93 ± 8	100 ± 5	*

[1] Average numbers of MB-derived cells that migrated in transwell assays towards different concentrations of examined growth factors. Values were experimentally measured and are shown with mean and standard deviation.

* denotes growth factor concentrations not measured in the current study.

Table 2

Summary of migration parameters for EGF and SDF-1.[2]

Migration Parameters	EGF	SDF-1
Fraction of motile cells (f) [%]	72.8%	67.3%
Cell Directionality (D) [%]	61.6%	44.2%
Average Maximum Cell Path Length (PL) in μm [Mean ± SD]	264.5 ± 67.9 μm	125.5 ± 48.6 μm

[2]Migratory parameters of MB-derived cells along the *μ*Lane system in response to concentration gradients generated by 100ng/mL of EGF and 100 ng/mL of SDF-1, respectively. Values were experimentally measured and shown as percentages, means and standard deviations. (n_{cells} ~ 180 cells for each ligand).

Table 3

Summary of migration parameters in response to gradient fields of EGF and SDF-1.[3]

	EGF Gradient Fields					SDF-1 Gradient Fields				
Migration Parameters	**G_1**	**G_2**	**G_3**	**G_4**	**G_5**	**G_1**	**G_2**	**G_3**	**G_{G4}**	**G_5**
Fraction of motile cells (f) [%]	28.3	18.6	11.9	10.3	3.7	18.2	20	13.8	8.7	6.5
Cell Directionality (D) [%]	28.3	15	7	8.6	2.7	18.4	10.5	9.8	2.2	3.3
Average Cell Path Length (PL) in μm [Mean ± SD]	281 ± 21	267 ± 40	226 ± 23	284 ± 28	389 ± 20	154 ± 34	114 ± 39	124 ± 42	94 ± 18	127 ± 37

Figure 1, Rico, CMB

[3]Migratory parameters of MB-derived cells in response to gradient fields, G_1-G_5, generated by of 100ng/mL of EGF or SDF-1 along the μLane system, respectively. Fraction (f) and directionality (D) of motile cells shown as percentages of total cell numbers. Average maximum cell path lengths (PL) shown with mean and standard deviation. (n_{cells} ~ 180 cells for each ligand).